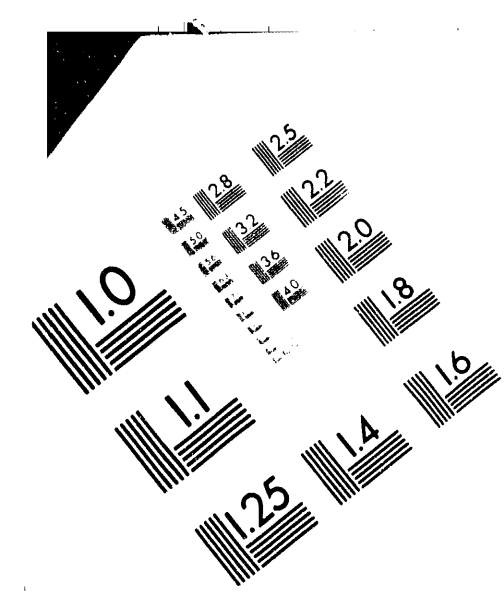

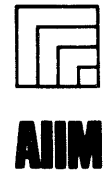

Association for Information and Image Management

1100 Wayne Avenue, Suite 1100
Silver Spring, Maryland 20910

301/587-8202

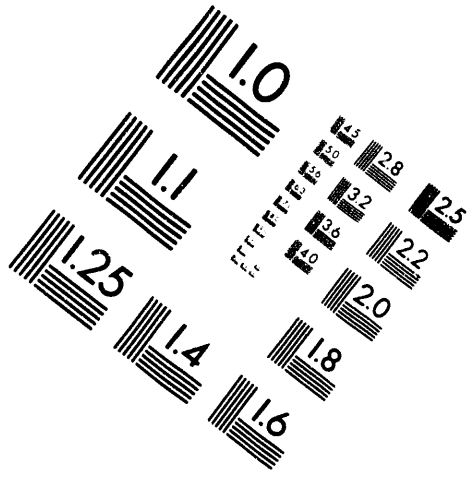

Centimeter

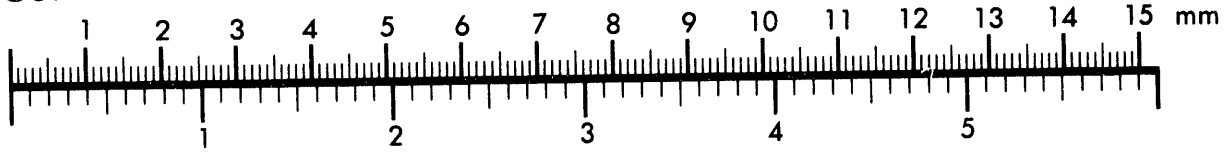

Inches

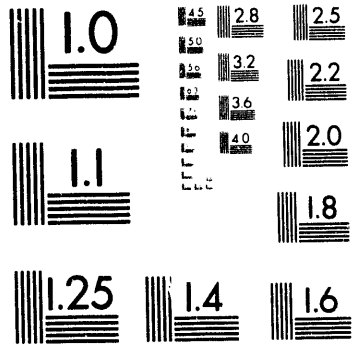

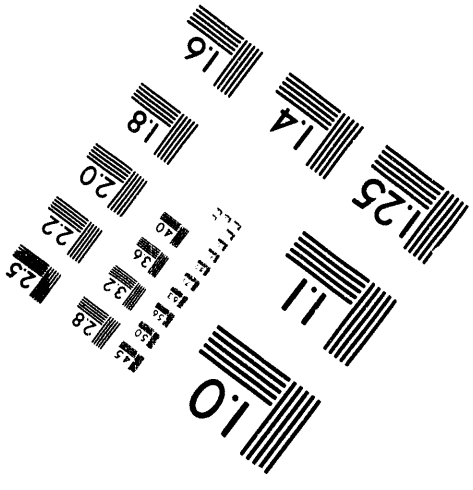

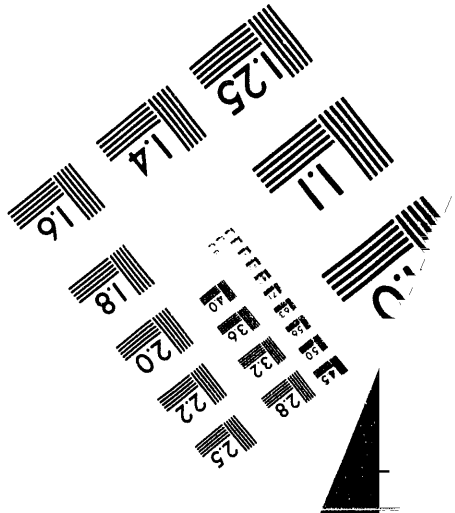

MANUFACTURED TO AIIM STANDARDS
BY APPLIED IMAGE, INC.

1 of 1

Procedures for Measuring the Properties of Heat-Pipe Wick Materials

Douglas R. Adkins and Ronald C. Dykhuizen
Sandia National Laboratories, Albuquerque, NM, 87185-5800

Accurate measurements of wick properties must be available to design high-performance heat pipes and to properly interpret results from heat pipe tests. In a program that is aimed at developing heat-pipe receivers for solar-Stirling electric systems, we have recently explored procedures to measure the effective pore radius and permeability of wick materials in their final "as fabricated" condition. Measurement techniques are compared in this paper and problems that are frequently encountered in measuring wick properties are discussed.

Wick Properties

For the low Reynolds number flows encountered in heat pipe wicks, the pressure drop through the wick can be determined using Darcy's equation,

$$\nabla P = \frac{\mu v}{\kappa} - \rho \mathbf{a}, \qquad (1)$$

where μ is the dynamic viscosity (kg/m·s), v is the superficial velocity (m/s), κ is the wick permeability (m^2), ρ is the density (kg/m^3), and $\mathbf{a}$ is the acceleration (=1g for a stationary wick). Capillary forces that help transport liquid through the wick are given by the expression,

$$\Delta P_c = \frac{2\sigma\cos\theta}{r_e}, \qquad (2)$$

where σ is the surface tension at the liquid vapor interface (N/m), θ is the contact angle, and r_e is the effective pore radius of the wick (m). ΔP_c is the pressure drop across the meniscus at the liquid gas interface (Pa).

The flow related characteristics of the wick are primarily defined by the permeability, κ, and the effective pore radius, r_e, and the contact angle, θ. Empirical correlations for κ and r_e are provided in several sources such as Brennan and Kroliczek [1979], Dunn and Reay [1983], and Chi [1972]. These correlations, however, are rather general so the predicted properties can be in error by a factor of three or more. The empirical correlations also do not account for the deformations that occur during the fabrication process. For more accurate results, the properties must be measured directly on the finished product.

Methods to measure the flow properties of wicks are described in papers by Freggens [1968] and Phillips and Hinderman [1969]. Brennan and Kroliczek [1979] also offer a comprehensive discussion of measuring wick properties. A recent paper by Adkins and Moss [1990] built upon this earlier work to develop simple procedures for measuring the properties of wicks in final fabricated conditions. This current paper continues to explore techniques for measuring wick properties, and it describes sources of errors that can affect measured results.

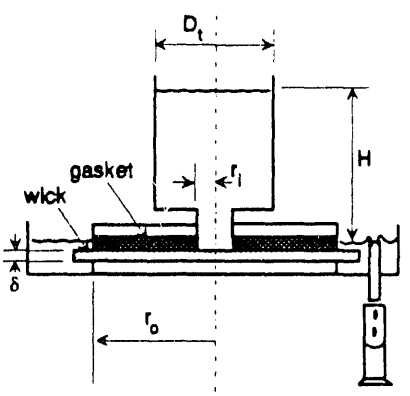

Fig. 1. System for forced-flow permeability measurements.

Forced-Flow Permeability Measurements

Permeability can be determined in a straight-forward manner by forcing liquid through the wick structure while measuring the pressure drop and the flow rate. For the system illustrated in Fig. 1, the fluid enters at the center of the circular test fixture and flows radially through the wick structure to the outer edge. If the flow is assumed to be 1-D in the radial direction, then Darcy's equation (EQ 1) for the pressure gradient becomes,

$$\frac{dP}{dr} = \frac{-\mu u_r}{\kappa} = \frac{-\mu \dot{V}}{2\pi r \kappa \delta}, \qquad (3)$$

where V is the volumetric flow rate through the wick (m^3/s), r is the radial position in the wick (m), and δ is the wick's thickness (m). By integrating from where fluid enters the wick (r_i) to where fluid exits the wick (r_o), EQ 3 can be solved for the wick permeability,

$$\kappa = \frac{v \dot{V} \ln(r_o / r_i)}{2\pi g H_L \delta}, \qquad (4)$$

DISCLAIMER

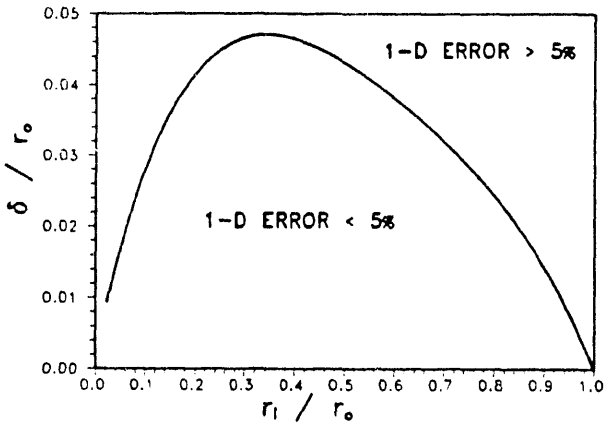

Fig.2. Constraints on 1-D applicability of measurement system in Fig.1.

where ν is the kinematic viscosity (m^2/s) and H_L is the head loss between the inlet and the exit of the wick ($\approx$ H in Fig.1). To apply EQ 4 in this form, it is assumed that the supply tube is large enough that H remains relatively constant during the test.

EQ 4 was used by Adkins and Moss [1990] to determine the permeability of several screen wick structures. Since that time, however, problems have arisen when EQ 4 was applied to systems where the 1-D assumption is invalid. This assumption can be violated when the inner radius is small or the wick is thick enough that the pressure drop developed as fluid enters the wick cannot be ignored. To determine when the 2-D effects should be considered, the simple 1-D model of EQ 4 can be compared to the 2-D solution of EQ 1. By taking the divergence of Darcy's equation, EQ 1 becomes

$$\nabla^2 P^* = \frac{\mu}{\kappa} \nabla \cdot v \ , \qquad (5)$$

where P^* is defined as $P - \rho g z$. From continuity considerations for an incompressible fluid, the right-hand side of EQ 5 is zero. For a 2-D flow in the radial and axial directions, EQ 5 becomes

$$\frac{1}{r}\frac{\partial}{\partial r}\left(r \frac{\partial P^*}{\partial r} \right) + \frac{\partial^2 P^*}{\partial z^2} = 0 \ . \qquad (6)$$

EQ 6 was solved for the pressure distribution using a 2-D spectral-element partial differential equation solver [NEKTON 1992] with the boundary conditions $P^*=H$ across the inlet surface of the wick, $P^*=0$ across the outlet surface of the wick, and $\partial P/\partial z=0$ over all other surfaces of the wick. EQ 1 was used to determine the velocity profile and the total flow rate through the wick. It should be noted that the pressure distribution predicted by EQ 6 depends only on the pressure head, H, which appears in the boundary conditions.

In Fig.2, the 2-D solution of EQ 1 and EQ 6 is compared with the 1-D analytical solution (EQ 4). The 1-D solution will always under-predict the permeability, but the estimates will be within 5% of the 2-D solution for systems where the nondimensional wick thickness, δ / r_o, for the given inlet radius, r_i/r_o, lies beneath the curve in Fig.2. Inaccuracies in the 1-D predictions can arise when the wick is very thick or the inner radius approaches zero or r_i. In these cases, the 2-D aspects of the flow will dominate in the system.

For a system that fits the criteria of Fig.2, conditions at the outer edge of the wick sample will, in general, have little impact on permeability predictions. In comparison to the velocities at the inner radius, velocities at the outer radius are small and, therefore, the pressure gradients in this area are also small. As long as flow from the wick surface is unimpeded a short distance from r_o, and the wick is saturated (so surface tension does not influence the flow), the answers obtained using EQ 4 will be reasonable.

For the situation where the liquid column shown in Fig.1 decreases significantly during a test, EQ 4 can be corrected to account for this drop in supply pressure. Assuming that the flow through the wick is quasi-steady, EQ 4 can be used to determine the instantaneous flow rate,

$$\dot{V} = -\frac{\pi D_t^2}{4}\frac{dH}{dt} = \frac{2\pi g \delta \kappa}{\nu \ln(r_o / r_i)} H \ , \qquad (7)$$

where D_t is the diameter of the inlet supply tube. By integrating EQ 7 from time t_1 to t_2, the permeability of the wick is found to be

$$\kappa = \frac{\nu D_t^2 \ln(H_1 / H_2) \ln(r_o / r_i)}{8 g \delta (t_2 - t_1)} \ , \qquad (8)$$

where H_1 and H_2 are, respectively, the initial and final heights of liquid in the supply tube.

In the current receiver development program, the wick structure is applied to the convex surface of a spherical dome. A system similar to the one pictured in Fig.1 can be used to determine the permeability of the wick. Following the steps used to derive EQ 8, the permeability of the wick is given by

$$\kappa = \frac{\nu D_t^2 \ln\left(H_1/H_2\right)}{8 g \delta (t_2 - t_1)} \ln\left[\frac{r_o\left(R + \sqrt{R^2 - r_i^2}\right)}{r_i\left(R + \sqrt{R^2 - r_o^2}\right)} \right] ,$$

where R is the radius of the dome, r_i is the radius at the fluid inlet and r_o is the radius at the outlet.

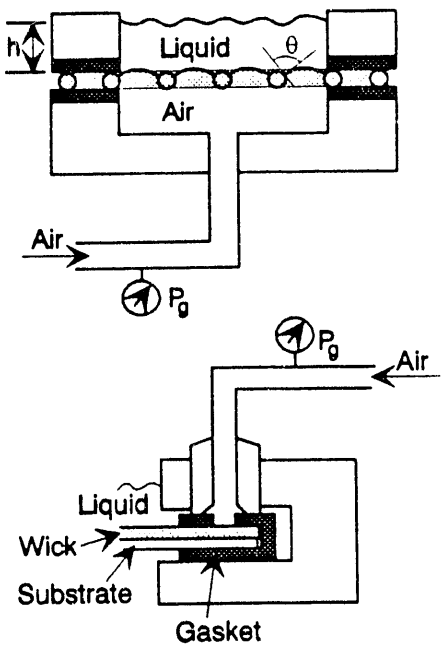

Fig.3. Bubble-point system for measuring the effective-pore radius. The option at the bottom is used when the wick is mounted on a substrate.

Bubble-Point Pore Radius Measurements

The dimensions of the pores along the liquid vapor interface will determine the capillary pumping capabilities of the wick. An estimate of the effective pore radius of a wick can be made by measuring the gas pressure that a wick can support when it is covered with liquid. This is sometimes referred to as the air entry pressure.

Two systems for measuring the effective pore radius are illustrated in Fig.3. In both systems, air is forced into the wick until bubbles appear on the surface. The pressure measured in the air space indicates the pressure difference that can be supported by the meniscus at the liquid vapor interface. Based on this retention pressure, the effective pore radius can be derived from EQ 2 as

$$r_e = \frac{2\,\sigma\cos\theta}{P_g - \rho g h}\,, \qquad (9)$$

where P_g and h are defined in Fig.3. By using the bubble-point test there is an implicit assumption that the wick can be characterized by a single pore size. In reality, each wick has a range of pore sizes and this artifact influences how the wick properties must be interpreted. The maximum capillary pressure a wick can provide is characterized by the smallest pore size and the air entry pressure is governed by the largest pore networks within the wick. However, the largest pore is of interest in developing conservative designs.

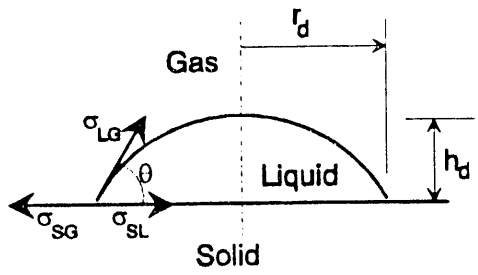

Fig.4. Interfacial tension forces.

The contact angle, θ, is determined by the balance of interfacial tension forces acting on the junction as indicated in Fig.4. This balance of forces is described by Young's equation,

$$\cos\theta = \frac{\sigma_{SG} - \sigma_{SL}}{\sigma_{LG}}\,, \quad 0 < \theta < 180^\circ\,, \qquad (10)$$

where σ_{SG}, σ_{SL}, and σ_{LG} ($\sigma_{LG}=\sigma$ in EQ 9) are the effective interfacial tensions illustrated in Fig.4. Interfacial tensions are a result of the discontinuity of intermolecular forces that exists at free surfaces of materials. In practice, interfacial tensions at solid surfaces are not measured directly, but the concept expressed in Young's equation is useful in explaining how the contact angle can be altered. For instance, a nonvolatile surfactant that is absorbed by the liquid and lowers σ_{LG} will reduce the contact angle. Similarly, a film of oil or wax with a lower σ_{SV} may cause a greater apparent contact angle. Reactions between the liquid and solid may reduce σ_{SL} and improve the wetting [Reed 1988]. Surface roughness will also reduce the apparent contact angle [Adamson 1990].

A zero contact angle (i.e., $\sigma_{SG} \geq \sigma_{SL}+\sigma_{LG}$) implies that the liquid will spread-over and completely wet the solid surface. Liquid metals, such as sodium, usually have good wetting characteristics on a clean metal surfaces [Cottrell 1964]. Fluids used to measure wick properties, however, may not have a contact angle of zero with a wick material.

To estimate the wetting capability of the wick, a small drop of the test fluid can be placed on a flat surface that is made of the same material as the wick in roughly the same condition. As shown in Fig 4, the height of the drop, h_d, in relation to the contact radius of the drop, r_d, gives an indication of the contact angle through the expression

$$\tan(\theta/2) = h_d / r_d\,, \qquad (11)$$

for $\theta < 90^\circ$ [Adamson 1990]. If the drop has a diameter that is roughly 12 times its height, then the error introduced by setting $\cos\theta = 1$ in EQ 9 will be about 5%.

Rate-of-Rise Property Measurements

Both the permeability and the pore radius can be estimated by observing the rate at which liquid rises through a wick. This technique, which is sometimes referred to as the blotter experiment, is discussed in a number of papers [Bell and Cameron, 1906, Ambrose and Chow, 1990, Bean, Bubb, and Fanelli, 1991]. A related phenomena in capillary tubes has also received considerable attention [Washburn, 1921, Brittin, 1945, Ligenza and Bernstein, 1951, Peiris and Tennakone, 1980].

Ligenza and Berstein [1951] demonstrated that the rate-of-rise approach works well in modeling flow through capillary tubes, but both Brennan and Kroliczek [1979] and Bean, Bubb and Fanelli [1990] claim that blotter experiments only give order-of-magnitude estimates of capillary spaces in porous materials, but a comparison of wick properties measured through different techniques is not provided. Even though order-of-magnitude results will not be acceptable in many cases, the simplicity of this approach does make it of interest. The rate-of-rise technique also accounts for the reduced flow cross-section in the wick that results when the liquid meniscus recedes into the wick's surface, so it may yield results that are more representative of the wick flow encountered in working heat-pipes. In addition, the rate-of-rise technique can easily be applied to curved wick structures.

Figure 5 illustrates the basic test system for the capillary rise experiment. Once the wick sample is brought in contact with the liquid, the distance that the front travels is recorded as a function of time. As the liquid advances through the wick, the pressure gradient in the liquid is described by Darcy's law as

$$\frac{dP}{dz} = -\frac{\mu v}{\kappa_w} - \rho g \sin\beta \,, \tag{12}$$

where β is defined in Fig.5 and the other terms are defined in EQ 1. The superficial velocity (or volumetric flux), v, can be related to the observed front velocity, V_f, through the expression

$$v = \varepsilon V_f = \varepsilon \frac{dZ_f}{dt} \,, \tag{13}$$

where ε is the porosity and Z_f is the location of the moving front [Bird, Stewart and Lightfoot, 1960].

By integrating the pressure gradient term in EQ 12 from the surface of the pool to the leading edge of the moving front, the pressure difference in the liquid is given as

$$P|_0 - P|_{Z_f} = -\left(\frac{\varepsilon \mu}{\kappa}\right) Z_f \frac{dZ_f}{dt} - (\rho g \sin\beta)\, Z_f \,, \tag{14}$$

The pressure difference on the left-hand side of EQ 14 is assumed to be equal to the maximum capillary pumping pressure given in EQ 2. EQ 2 and EQ 14 can be combined to give

$$Z_f \frac{dZ_f}{dt} = V_m (H_m - Z_f) \,, \tag{15}$$

where,

$$H_m = \frac{2\sigma\cos\theta / r_e}{\rho g \sin\beta} \,, \text{ and } V_m = \frac{\kappa}{\varepsilon} \frac{g \sin\beta}{\nu} \,.$$

Physically, H_m is the maximum height that liquid can rise through the wick by capillary pumping, and V_m is the velocity liquid would flow down the wick if frictional losses equaled the hydrostatic head.

Normally, the location of the front is measured as a function of time and a plot is made of dZ_f/dt vs. $1/Z_f$. In accordance with EQ 15, this curve should be a straight line and the permeability and pore radius can be obtained from the slope and intercept of line [Brennan and Kroliczek 1979]. EQ 15 can, however, be integrated to yield

$$-V_m t = Z_f - Z_0 + H_m \ln\left(\frac{H_m - Z_f}{H_m - Z_0}\right) \,, \tag{16}$$

where Z_0 is the front location at t=0, and Z_f is the front location at time t. The parameters V_m and H_m can be obtained by performing a least squares fit of EQ 16 on measured rate-of-rise data. The permeability and pore radius can be obtained from the definitions of H_m and V_m given in EQ 15.

In developing EQ 15, evaporation of liquid from the wick surface was ignored. If liquid evaporates from the wick surface, the motion of the liquid front will no longer indicate the total flow rate through the wick. Evaporation also tends to cool the liquid in the wick and alter the

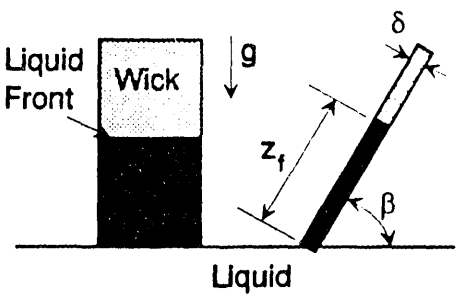

Fig.5. Rate-of-rise system for measuring permeability and effective pore radius.

fluid's viscosity and surface tension. To some extent, the property changes tend to cancel; increased pressure drops that are caused by increases of viscosity are offset by the increases in capillary pumping that occur as the surface tension increases. Evaporation rates can be estimated by measuring combined weight changes in the wick sample and the test fluid. In this study, however evaporation rates will simply be recognized as a source of error, and no attempt will be made to model the impact on property measurements.

The possible dependency of the contact angle on the flow rate is another factor that was ignored in the above derivation. Blake and Haynes [1967] demonstrated that models based on EQ 2 work best in predicting capillary tube flows for a receding flow and worst when the liquid is advancing through a capillary. It is generally argued that the discrepancy is caused by changes in the contact angle, θ, with velocity. Joos, Remoortere, and Bracke [1990] developed an expression that correlates the contact angle to the velocity of the advancing liquid in a capillary tube, but it is not known if this correlation can be applied to wick structures, so it has not been applied to the current rate-of-rise model. The theory that was used to derive EQ 16 also assumes that the wick becomes 100% saturated as the front passes. This is not always true, particularly in wicks with large variations in pores.

Experimental Measurements

Property measurement tests were performed on several wick samples, but only two representative cases will be presented here. Both samples were formed by vacuum sintering layers of 316 stainless steel screens in a furnace for two hours at 1050°C. After the screens were removed from the sintering fixture, they were cleaned in an ultrasonic bath with water and then rinsed in methanol and allowed to thoroughly dry. The edges were then trimmed to form 83x83 mm square samples. The samples are described in Table 1.

Forced-Flow Experiments: Permeability was first measured by forcing liquid to flow through the wick with the system that is shown in Fig.1. In the system used, r_i=3/4" (19mm), r_o=3" (76mm), and D_t=1/4" (6.35mm). For these dimensions, wicks up to 2-mm thick are well within the range where the 1-D flow assumption is valid (see Fig.2). Permeability tests were performed using 2-propanol as the working fluid. Viscosity measurements that were made on the fluid after the tests are given in Table 2.

To avoid trapping bubbles in the wick specimens, the test fixture was submerged in propanol and the samples were soaked and then loaded under the fluid surface. A neoprene gasket was placed between the fixture and the wick sample to insure that any small distortions in the wick did not provide alternate paths for the flow. The gasket was covered with aluminum foil to prevent neoprene from embedding in the wick.

Table 1. Screen Wick Dimensions

Mesh (wires/in)	Wire ϕ (μm)	number layers	thickness, δ (mm)
200x200	53.3	8	0.66±0.01
325x325	35.6	8	0.57±0.02

Table 2. Properties of 2-Propanol

T (°C)	ρ^* (kg/m^3)	ν^* (m^2/s)	σ^{**} (N/m)
23	---	2.82×10^{-6}	0.0236
24	781.6	---	0.0235
25	---	2.69×10^{-6}	0.0234

*measured properties
** interpolated values [Weast 1975]

Fluid was drawn up the 1/4" (6.35 mm) diameter supply tube with a vacuum to approximately 14" (36 cm) above the pool. Time and location measurements were then recorded as the liquid fell from 12.5" (31.75 cm) to 2.5" (6.35cm) above the pool. These measurements are shown in Fig.7. The permeability of the samples was calculated with EQ 8 using the start and stop times of the tests and the fluid property values in Table 2. The correlation based on EQ 8 and the predicted permeabilities are illustrated in Fig.6. These tests were very repeatable and the correlation with EQ 8 appears to be good. Permeabilities that were determined from the forced flow experiments are listed in Table 3. The porosity (or void fraction) in Table 3 was calculated using the volume of the screen (based on the sample weight and stainless steel density) and the total volume of the sample (based on the overall dimensions).

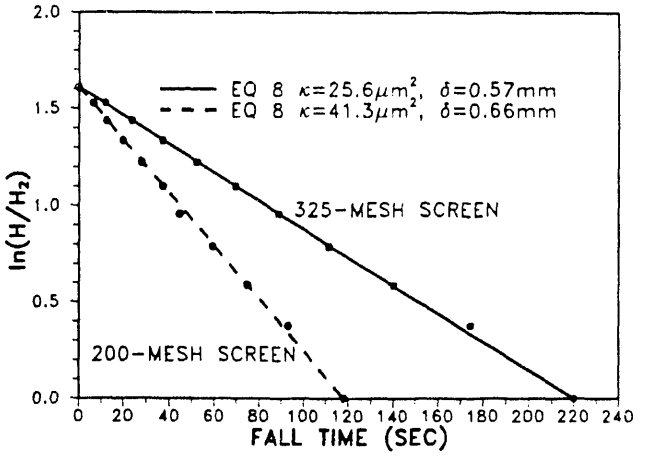

Fig.6. Descent rate for liquid column in permeability fixture shown in Fig.1.

Bubble-Point Tests: Pore radius measurements were made with both of the fixturing options shown in Fig.3. Air was first forced to flow through the wick to insure that the air-liquid interface was at the surface and not within the wick. (In the wick flow models it is assumed that liquid flows through the entire thickness of the wick, so the effective pore radius on the wick's surface is of the most interest.) After air flowed from the surface, the pressure was lowered until the bubbles no longer departed from the surface and then the pressure was increased to determine the maximum pressure achievable before bubbles would again depart from the surface. The effective pore radius that was calculated using the measured bubble retention pressure in EQ 9 is given in Table 3. The measurements were repeatable for both of the samples and the results were not affected by the fixturing option selected to force air into the wick (see Fig.3).

For the effective pore radii presented in Table 3, it was assumed that the contact angle equaled zero. To test this assumption, a small drop of 2-propanol was placed on a strip of 316-SS that had undergone the same heat treatment and cleaning as the screens. The drop spread out to a 24-mm diameter and the height was less than 1 mm. The zero contact angle assumption was probably reasonable for this system. For comparison, a small drop of water was placed on the surface, and the measured contact angle was approximately 53° based on the drop height, the contact diameter, and EQ 11.

Rate-of-Rise Tests: Rate-of-rise experiments were performed by attaching a scale to the screen and measuring the time required for liquid to travel up the surface. The front immediately begins to move up the surface as the wick contacts the liquid, so time measurements were not made until the front was slightly more than 1 cm above the pool surface. For the 325-mesh screen, the front was fairly uniform across the wick and it was possible to measure its location within ±2 mm. In contrast, the front was irregular across the wick surface with the 200-mesh sample; at times, the front would skew to one side and, at other times, streaks would emerge during the test and travel about one centimeter ahead of the front.

Data from two trials with the 325-mesh screen are shown in Fig.7. As the data shows, the general trends were the same in the two runs, but liquid did travel faster through the wick in the second run. The higher flow rates could be attributed to several factors. Residual liquid in the wick would make it appear that liquid was traveling faster through the wick, however, this problem was anticipated so the wick was dried thoroughly in air before each test was performed. The higher temperature of the second run would cause a 5% drop in the viscosity and only 1% drop in the surface tension so the net effect would be to accelerate flow through the wick. Errors in

Table 3. Measured Screen Wick Properties

Mesh (wires/in)	ε (%)	κ (μm^2)	r_e (μm)
200	57.7	41.3±0.7	49±1
325	63.5	25.6±1.0	33±1

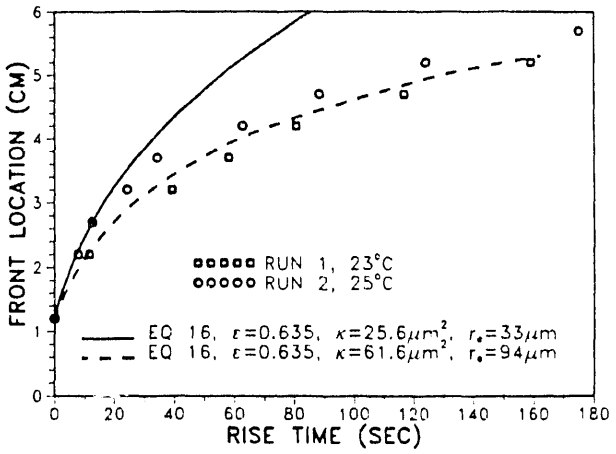

Fig.7. Rate of liquid rise in 325-mesh screen wick.

the identifying the location of the liquid front could also contribute to the differences between the two runs.

EQ 16 was used to predict the location of the front as a function of time and these results are shown as solid and dashed lines in Fig.7. The solid line is based on the previously measured values of κ, ε, and r_e in Table 3. The dashed line was obtained by performing a least-squares fit on the data in Fig.7 to solve for the coefficients of EQ 16. Agreement between the model and the experiments appears to be poor when the earlier values for wick properties are used in EQ 16. As might be expected, the agreement improves when the data are used to determine the coefficients of EQ 16, but predicted values for permeability and pore radius are larger than those measured through forced flow and bubble tests.

For the properties listed in Table 3, the theory and the experiment coincide only during the initial stage of the test. Neglected factors, such as evaporation and falling temperatures, would cause the front velocity to decrease during the test. Including these factors in a model, however, will not be simple, because new parameters, such as the evaporation rate from the surface, will be introduced. The sensitivity of the predictions to the measured data also makes the rate-of-rise results questionable. For instance, there is only about a 4-mm difference between RUN 1 and RUN 2 in Fig.7 at any selected time. This small difference, however, changes the prediction from κ=42 μm^2 for the data in RUN 1 to κ=73 μm^2 for the data in RUN 2. In other words, a 4-mm error in locating the front can cause a 80% error in the predicted permeability.

Summary and Conclusions

Accurate property data are needed to develop wick structures for high-performance heat pipes. In most cases, empirical correlations are too general to provide this information. The properties can be determined through direct measurements, however, even measured results can have large errors for some tests procedures.

A wick's permeability can be measured by forcing liquid to flow radially through the wick and measuring the pressure drop as a function of flow rate. This procedure is simple to use and it yields repeatable results. Precautions must be taken, however, to insure that flow is not impeded by bubbles in the wick, and the surface of the wick must be flooded to avoid the influence of capillary forces at the exit surfaces of the wick. To use a simple 1-D flow approximation, the test fixture must be designed to give the greatest pressure drop through the radial-flow portion of the test system; pressure drops at the inlet of the wick should be minimized. Simple design parameters for the test fixture are given in Fig.2.

The effective pore radius can be estimated by measuring the air entry pressure for a wick submerged in a liquid. A liquid that wets the wick material well (such as alcohols on stainless steels) should be used to avoid the effects of a non-zero contact angle. The bubble-point tests provide repeatable measurements of the effective pore radius, however, constrictions in the wick can cause variations in the effective pore radius within the wick.

Both the permeability and the effective pore radius can be estimated by measuring the rate liquid travels up the wick by capillary pumping. Several factors, such as evaporation and difficulties in locating the liquid front, can make this procedure difficult to apply. In practice, it was found that this procedure was not very repeatable and the results did not correspond well with the measurements obtained with other procedures.

Acknowledgments

The authors would like to thank Steve Rugg for his assistance in programming, and Louis Gritzo for his work on the 2-D flow model. This work was performed at Sandia National Laboratories which is supported by the Department of Energy under contract DE-AC04-76DP00789. Sandia document number SAND92-2347C.

References

Adamson, A.W., *Physical Chemistry of Surfaces*, 5th ed., John Wiley & Sons, NY, **1990**.

Adkins, D.R., and T.A. Moss, "Measuring Flow Properties of Wicks for Heat Pipe Solar Receivers," *Proceedings of the ASME Solar Engineering Conf.*, Miami, FL, April **1990**.

Ambrose, J.H., L.C. Chow and J.E. Beam, "Capillary Flow Properties of Mesh Wicks," *J. Thermophysics and Heat Transfer*, Vol. 4, No. 3, pp 318-324, July **1990**.

Bean, C.P., J.I. Bubb, D.F. Fanelli, "Fluid Up-take by a Blotter," *Am. J. Phys.*, Vol. 59, No. 6, pp 533-535, June **1991**.

Bell, J.M., and F.K. Cameron, "The Flow of Liquid through Capillary Spaces," *J. Phys. Chem.*, Vol. 10, pp 658-674, **1906**.

Bird, R.B., W.E. Stewart, and E.N. Lightfoot, *Transport Phenomena*, pp 197, John, Wiley & Sons, Inc., NY, **1960**

Blake, T.D., D.H. Everett, and J.M. Haynes, "Wetting," SCI Monograph No. 25, Society of Chemical Industry, London, **1967**.

Brennan, P.J.,and E.J. Kroliczek, "Heat Pipe Design Handbook: Vol. 1," NTIS Pub. No. N81-70112, June **1979**.

Britten, W.E., "Liquid Rise in a Capillary Tube,"*J. of Appl. Phys.*, Vol. 17, pp 37-44, January **1946**.

Chi, S.W., **Heat Pipe Theory and Practice: A Source-book**, Hemisphere Publishing Corp., Washington, DC, **1972**.

Cottrell, A.H., *The Mechanical Properties of Matter*, John Wiley & Sons, Inc., New York, **1964.**

Dunn, P.D., and D.A. Reay, **Heat Pipes**, 3rd ed., Pergamon Press, Oxford United Kingdom, **1983**.

Freggens, R.A., "Experimental Determination of Wick Properties for Heat Pipe Applications," *Proceedings of the 4th IECEC*, Paper 699108, pp 888-897, **1968**.

Joos, P., P. Van Remoortere, and M. Bracke,"The Kinetics of Wetting in a Capillary," *J. of Colloid and Interface Science*, Vol. 136, No. 1, pp 189-197, April **1990**.

Ligenza, J.P., and R.P. Berstein, "Rate of Rise of Liquids in Fine Vertical Capillaries," *J. Am. Chem. Soc.*, Vol. 73, pp 4636-4638, **1951**.

NEKTON User's GuideVersion 2.85, Fluent Inc., Lebanon, NH, **1992**.

Peiris, M.G.C., and K. Tennakone, "Rate of Rise of a Liquid in a Capillary Tube," *Am. J. Phys.*, 48(5), pp 415, May **1980**.

Phillips E.C., and J.D. Hinderman, "Determination of Properties of Capillary Media Useful in Heat Pipe Design," *Proceedings of the ASME-AICHe Heat Transfer Conf.*, Paper No. 69-HT-18, Minneapolis, MN, Aug. **1969**

Reed, J.S., *Introduction to the Principles of Ceramic Processing*, John Wiley & Sons, New York **1988**.

Washburn, E.W., "The Dynamics of Capillary Flow," *The Physical Review*, 2nd Series, Vol. XVII,, No. 3, pp 273-282, March **1921**.

Weast, R.C., *Handbook of Chemistry and Physics*, 55th ed., pp CRC Press, Cleveland, OH, **1975**.

DATE
FILMED
9/28/93
END